New Journal of Physics
An Institute of Physics and Deutsche Physikalische Gesellschaft Journal

Nanostructuration with visible-light-emitting silicon nanocrystals

F Huisken[1,2,5], D Amans[2], G Ledoux[2,6], H Hofmeister[3], F Cichos[4] and J Martin[4]

[1] Max-Planck-Institut für Astronomie, Königstuhl 17, D-69117 Heidelberg, Germany
[2] Max-Planck-Institut für Strömungsforschung, Bunsenstraße 10, D-37073 Göttingen, Germany
[3] Max-Planck-Institut für Mikrostrukturphysik, Weinberg 2, D-06120 Halle, Germany
[4] Institut für Physik, Technische Universität Chemnitz, D-09107 Chemnitz, Germany
E-mail: fhuiske@gwdg.de and friedrich.huisken@uni-jena.de

New Journal of Physics **5** (2003) 10.1–10.10 (http://www.njp.org/)
Received 6 November 2002
Published 31 January 2003

Abstract. Silicon nanocrystals with diameters between 2.5 and 7 nm were prepared by CO_2 laser pyrolysis of silane in a gas flow reactor. A small portion of the particles created in the reaction zone was extracted as a molecular beam through a conical nozzle and deposited at low energy on substrates. Placing suitable masks in front of the substrate, micro- and nanostructured films were obtained. The patterned structures were characterized by atomic force microscopy and transmission electron microscopy while their optical properties were studied by laser scanning confocal microscopy. Nanostructures as small as 30 nm could be produced. The photoluminescence emanating from a regular array of 1.2 μm sized dots composed of Si nanocrystals was studied with spatial, spectral and temporal resolution.

[5] Author to whom any correspondence should be addressed.
[6] Present address: LPCML, CNRS UMR 5620, Université Lyon I, F-69622 Villeurbanne, France.

Contents

1. Introduction

Due to strong visible photoluminescence (PL), first reported by Canham [1] and Lehmann and Gösele [2] more than ten years ago, porous silicon (p-Si) has become an attractive material with interesting applications in various fields ranging from optoelectronics to biology. The observation of efficient PL from an indirect semiconductor such as silicon was explained on the basis of quantum confinement leading to a widening of the bandgap and a partial relaxation of the selection rules making silicon a somewhat more direct-gap material [3, 4].

Very similar PL characteristics have been observed for silicon nanocrystals (nc-Si) [5, 6]. Compared to p-Si, Si nanocrystals have the advantage that they can be produced under chemically clean conditions as isolated non-interacting particles and that they can be selected according to their size [6, 7].

For several years, we have studied silicon nanoparticles produced by CO_2-laser-induced decomposition of silane in a gas flow reactor [6]–[8]. In the earlier studies, our interest was focused on their extraordinary optical properties which make them an attractive material for optoelectronic applications [9]–[11]. All results obtained in our laboratory could be explained on the basis of quantum confinement as the only process responsible for the observed properties. Further studies were devoted to the production of milli- and micrometre-sized patterned films being composed of light-emitting silicon nanoparticles [12, 13].

The present paper reports on recent achievements in the production of micro- and nanostructured films and their optical characterization using laser scanning confocal microscopy. Such investigations are a prerequisite for the development of silicon-based photonic crystals.

2. Sample preparation and experimental techniques

Crystalline silicon nanoparticles are produced via CO_2-laser-induced decomposition of silane in a dedicated gas flow reactor incorporated into a cluster beam apparatus [7, 8]. A schematic view of the major components is shown in figure 1. The radiation of a pulsed CO_2 laser interacts perpendicularly with the confined flow of silane (SiH_4) molecules emanating from a 3 mm diameter tube. The SiH_4 molecules are dissociated and a saturated vapour of silicon atoms at elevated temperature ($\geq$1300 K) is produced giving rise to condensation and subsequent growth of silicon nanoparticles. The as-prepared Si clusters are extracted from the flow reactor through a conical nozzle (a) of 0.2 mm diameter to form a pulsed molecular beam of non-interacting particles. Further shaping of the cluster beam is performed by a conical skimmer (b) of 1 mm diameter. Thin films of neutral silicon nanoparticles are obtained by placing a substrate (d) further

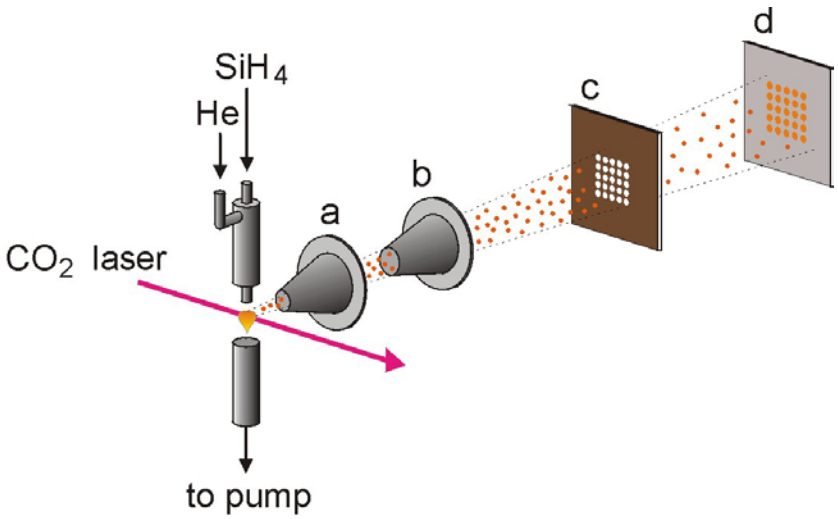

Figure 1. Schematic view of the set-up used for the preparation of structured films. A CO_2 laser is employed to decompose silane. Silicon nanocrystals are formed and extracted through a nozzle (a) and a skimmer (b) to form a collimated beam of freely propagating particles. A mask (c) is introduced into the beam so that a structured film can be deposited on the substrate (d).

downstream into the cluster beam. At this position the beam diameter is 7 mm. Structured films are obtained by mounting an appropriately structured mask (c) directly in front of the substrate. When the movable substrate and mask holder is not in place the particles can proceed into the following ultra-high vacuum chamber (not shown in the figure) where they are analysed by time of flight mass spectrometry (TOFMS) employing an ArF excimer for ionization. This gives us the possibility for an *in situ* determination of the size distribution of the silicon nanoparticles in the beam.

An extraordinary feature of the cluster beam apparatus is the possibility to select the Si nanoparticles according to their size by exploiting the correlation between velocity and mass, i.e. the fact that the larger nanoparticles are slower than the smaller ones. For this purpose, a standard molecular beam time-of-flight chopper with two 1 mm wide slits spinning with 400 Hz is placed between skimmer and mask (not shown in figure 1). If the CO_2 laser is properly synchronized with the chopper it is possible to select a narrow size distribution out of the much broader distribution arriving at the chopper. In this way, structured films of *size-selected* Si nanocrystals can be produced. The actual experimental parameters were as follows: flow of silane, 30 sccm; flow of helium, 1100 sccm; total pressure, 330 mbar; CO_2 laser line, 10 μP28 (936.8 cm^{-1}); laser energy, 30 mJ; pulse length, 20 ns; repetition rate, 20 Hz.

In the present study, size-selected or non-size-selected silicon nanoparticles were deposited at low energy on mica and quartz substrates. As masks, we used transmission electron microscopy (TEM) copper grids covered by holey carbon films as they are supplied for electron microscopy studies. The first holey carbon foil was a standard irregularly patterned film while the second one was regularly structured. The latter consisted of a matrix of 1.2 μm diameter holes whose centres were 2.5 μm apart (Quantifoil Micro Tools, Jena, model R1.2/1.3).

For the deposits on mica, we used atomic force microscopy (AFM) to characterize the structure of the deposit in the nanometre size regime (Digital Instruments Nanoscope III). The

TEM grid covered by the conventional holey carbon film was investigated by TEM using a JEM 1010 instrument operated at 100 kV. Hence, it was possible to compare finer details between mask and deposit. Silicon nanoparticles were deposited on quartz substrates to reveal the pattern of the deposit by optical means and to study the dynamics of the PL decay of the Si nanocrystals. For this purpose, a home-built sample scanning confocal microscope was used. The set-up follows the standard confocal layout. The emission in the confocal spot was collected using a $100\times/0.9$ NA microscope objective (Zeiss Epiplan) and finally detected by an avalanche photodiode. The excitation light was removed from the emission by an interference long-pass filter (Omega Optical). As exciting radiation, we used the 514.5 nm line of an argon ion laser. All measurements were performed under ambient conditions.

3. Structural characterization

The first deposition experiment was carried out in the size-selective mode using the irregular holey carbon film as a mask on top of a mica substrate. In this experiment, silicon nanoparticles with an average diameter of 3.9 nm and a full width at half maximum (FWHM) of 0.7 nm were allowed to fly through the holes of the carbon foil and to be deposited on the substrate. The other particles hitting the foil were prevented from reaching the substrate. As a result, the holey structure of the carbon foil was imaged on the substrate. The mica substrate was then analysed by AFM while the carbon film was characterized by TEM. A comparison of the images obtained for the corresponding samples with the different techniques is shown in figure 2. The left panel (a) reflects a low-resolution TEM image. One can easily recognize the various holes in the carbon foil which appear as light-grey areas. Some holes are bridged by filaments with typical diameters of 30 nm (see the filament marked by an arrow). All the carbon foil is covered by a dense layer of Si nanoparticles as will be shown below for the detail marked by the red rectangle (see figure 3). The right panel (b) of figure 2 shows the AFM image of the deposit on the mica substrate. The light areas present the regions covered by Si nanoparticles. Comparing with panel (a), it is seen that the holey structure of the carbon film is reproduced very well. Even finer details, for example the filament marked by an arrow in panel (a), can be clearly recognized.

If the mask or mica sample are illuminated by UV light from a mercury lamp ($\lambda = 254$ nm) intense red PL originating from the silicon nanocrystals can be observed with the naked eye [9, 13]. This visible PL results from the quantum nature of the nanosized Si crystallites. From the correlation between PL peak position and particle size [14], one can already conclude that the size of the crystallites is around 3.5 nm. The PL behaviour of an ensemble of size-selected Si nanoparticles has been studied in great detail before [6, 9, 11, 13]. These studies revealed that the strong visible PL can be solely explained on the basis of quantum confinement. Other PL mechanisms like surface states or defects need not be invoked.

The small area marked in figure 2 by the red rectangle is displayed in figure 3 with higher magnification. One can easily see that the filamentary structure of the carbon foil is closely packed by Si particles and one can easily distinguish the individual entities. Closer inspection reveals that the majority of nanoparticles have diameters between 4 and 5 nm. Earlier high-resolution TEM studies have shown that our Si nanoparticles are nicely crystalline and that they are surrounded by a layer of SiO_x whose thickness amounts to roughly 10% of the total diameter [15]. Thus, an average total diameter of 4–5 nm points to an average diameter of the crystalline core of 3.2–4 nm which is in nice agreement with the observation of PL by eye. A conventional optical microscope has been used to analyse the coarse structure of the light-

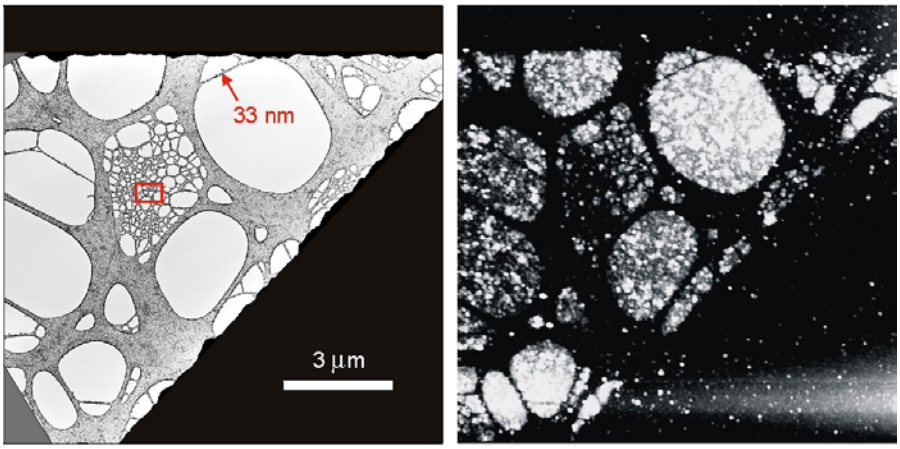

Figure 2. Comparison between the holey carbon film mask imaged by TEM (a) and the deposit on a mica substrate as imaged by AFM (b). The deposition time was 12 h.

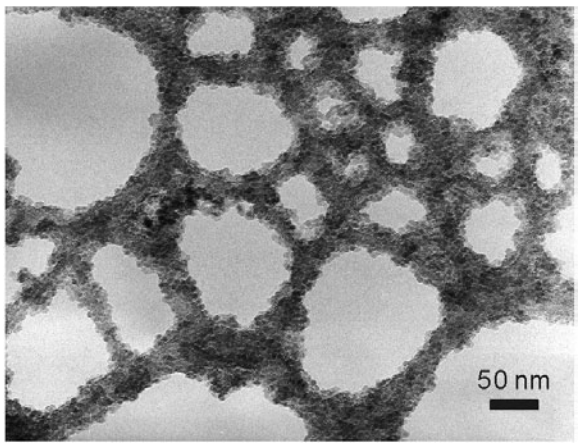

Figure 3. Detail of the TEM image marked in figure 2 by the small red rectangle. Individual Si nanoparticles with diameters between 3 and 5 nm can be recognized. The image size is 600 × 450 nm^2.

emitting layers [13]; however, more sophisticated methods must be used to reveal finer details (see below).

To obtain quantitative information about the structures of Si nanoparticles deposited through the mask on the mica substrate, further AFM studies were carried out. In figure 4, we present the height profile of a perpendicular cut through the shadow produced by the filament that is marked by the arrow in panel (a) of figure 2. The average thickness of the deposit is determined to be approximately 25 nm (for the 12 h deposition with size selection). On the other hand, the groove produced by the 33 nm thick filament and sampled by the AFM tip is 17 nm deep and approximately 70 nm wide. Although we have to keep in mind that this latter result is biased by the finite size of the tip we can conclude that the replica structure of the mask obtained on the mica substrate is rather sharp.

Proper determination of the thickness of a layer of Si nanoparticles is obtained by covering

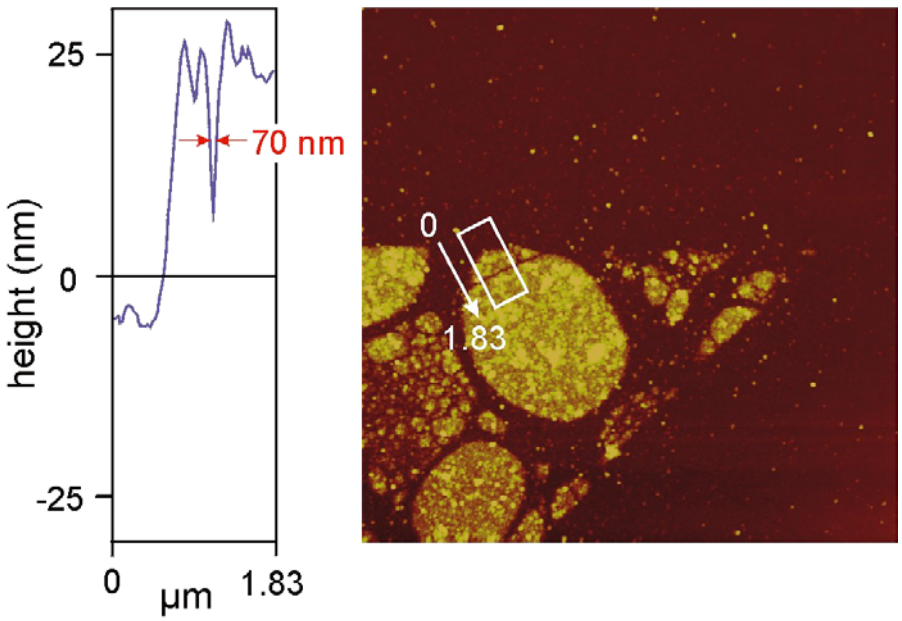

Figure 4. AFM study of a detail marked in figure 2 by an arrow.

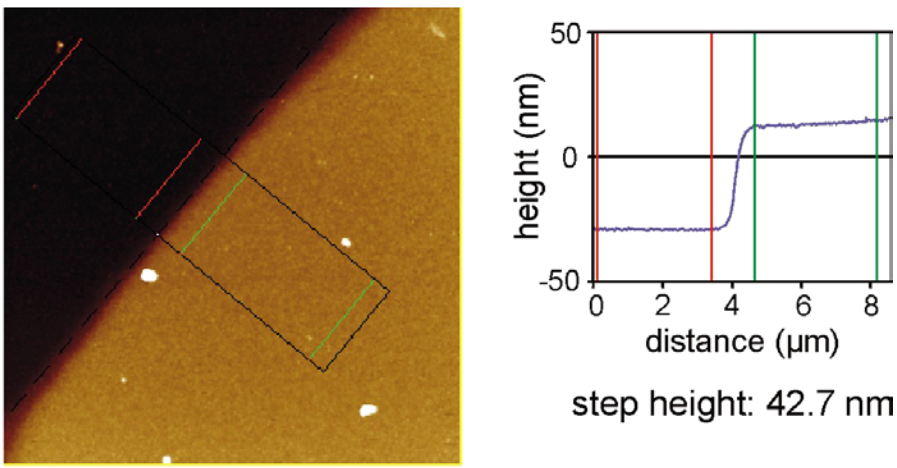

Figure 5. AFM image of a step produced by covering the mica substrate with a microscope cover slip before depositing the Si nanoparticles.

the flat substrate with a thin quartz microscope coverslip before depositing the particles. The analysis of a corresponding deposition experiment (6 h without size selection) is presented in figure 5. It reveals a very smooth surface of the deposited layer (light-brown area) and a rather sharp step with a width of 750 nm. Again we have to keep in mind that, due to the convolution with the finite size of the tip, the true step is actually sharper. In contrast, the height of the step is not influenced by this effect. Thus, we determine the thickness of the nanoparticle layer for a 6 h lasting deposit without size selection to be 42.7 nm.

In another deposition experiment, we have employed a regularly structured carbon foil as supplied by Quantifoil Micro Tools GmbH, Jena (model R1.2/1.3). It consists of a regular pattern of 1.2 μm holes 2.5 μm apart (separation between centres). The electron scanning

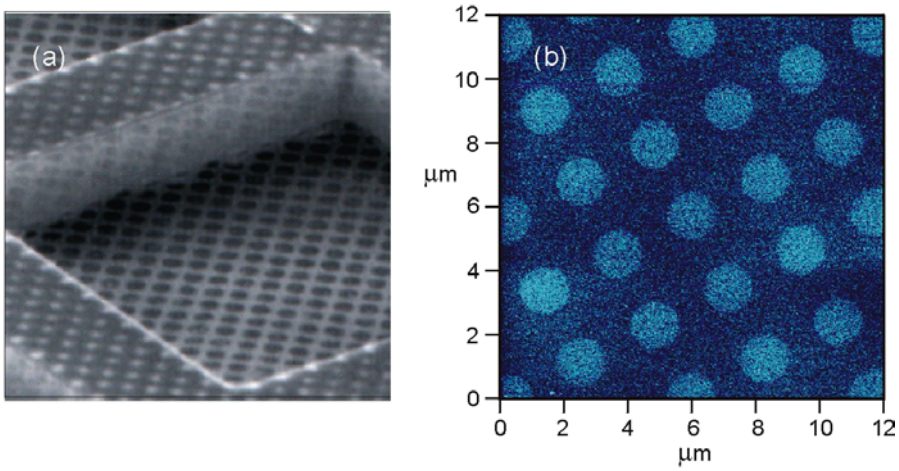

Figure 6. SEM micrograph of the R1.2/1.3 Quantifoil used as a mask in the deposition experiment (a). The right panel (b) shows the AFM image of the deposited structure of silicon nanoparticles ($12 \times 12\ \mu m^2$).

micrograph depicted in figure 6(a) shows the holey carbon foil and part of the copper support. Using this foil as a mask, we succeeded in producing a regular pattern of dots deposited on a mica substrate. The AFM image of this sample is reproduced in figure 6(b). The circular dots are made from approximately two monolayers of silicon nanoparticles with an average diameter of 3.25 nm. This and similar samples elaborated on quartz substrate have been used for optical characterization.

4. Optical characterization

The sample with the regular pattern of 1.2 μm dots was optically characterized using the home-built confocal microscope described in the experimental section. In figure 7 we present an image of the PL of the patterned sample. It should be noted that the individual 1.2 μm dots are clearly resolved and that the optical image agrees nicely with the SEM and AFM micrographs presented in figure 6. From this comparison, we can also conclude that the spatial resolution of the confocal microscope is of the order of 300 nm. The intensity of the PL is proportional to the height of the PL surface displayed in the figure.

In the following experiment, part of the sample containing four dots was irradiated by the 514.5 nm line of an argon ion laser ($P = 25.5\ \mathrm{kW\ cm^{-2}}$) for 1 min. The scan performed directly after this irradiation reveals a substantial decrease of the PL intensity for the Si nanoparticles subjected to the laser field that we will refer to as bleaching. We have also investigated the time dependence of this bleaching, and we observed a decay curve that cannot be described by a single exponential. Fitting stretched exponentials to the decay curves, we determined average time constants of the order of 1 s. The stretched exponential behaviour is indicative of a distribution of bleaching time constants. This distribution may be caused by the size distribution of the particles. Different sizes of the particles will result in different optical properties (e.g. different emission lifetimes) and thus also affect the time until photobleaching occurs. On the other hand, a distribution of bleaching time constants can also be caused by the existence of different bleaching mechanisms.

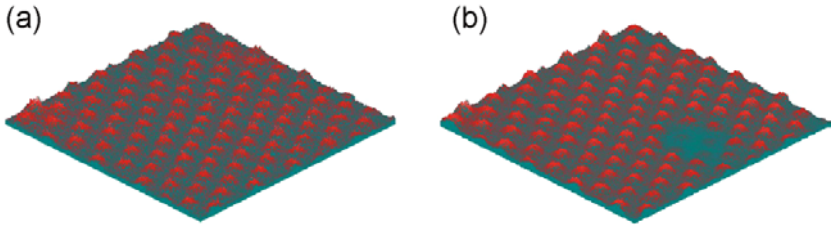

Figure 7. Confocal images of a pattern consisting of two monolayers of size-selected silicon nanoparticles before (a) and after (b) irradiation with the 514.5 nm line of an argon ion laser at 25.5 kW cm^{-2} for 1 min. The area is 20 × 20 μm^2.

To explore the mechanism of photobleaching in more detail, the PL arising from the Si nanoparticles has also been spectrally resolved. The combined spectral and temporal studies for a size-selected and non-size-selected sample are summarized in figure 8. For the size-selected sample (a), the initial PL response peaks at 650 nm. With progressive time, the PL intensity decreases (bleaching); but, in addition, the PL curve shifts to larger wavelengths (red shift). For the non-size-selected sample (b), this effect is much more pronounced. This is due to the broader size distribution and the resulting broader PL response. These observations can be interpreted as follows. If the bleaching is faster for the smaller particles than for the larger ones, with increasing time, the inhomogeneously broadened PL curve should experience a progressive red shift. Of course, this effect will be less pronounced for a sample with very narrow size distribution. Hence, from the observed spectral shifts, we can conclude that we have indeed a distribution of bleaching time constants which is correlated with the size distribution of the nanocrystals. If all particles possessed a similar lifetime for photobleaching no spectral shift would occur. However, even though the particle size distribution of the size-selected sample is rather narrow and the spectral shift during bleaching is very small, the nonexponential decay of the PL is still pronounced. Thus, the size dispersion cannot be the only reason for a nonexponential photobleaching. Indeed, a first analysis of the distribution of time constants observed in the present experiment shows at least two distinct peaks, indicating that at least two different bleaching mechanisms are operative. A more detailed analysis will be presented in a forthcoming paper.

The photobleaching can possibly be explained by the occurrence of Auger autoionization. If the laser intensity is sufficiently high, a second photon can be absorbed within the lifetime of the exciton created upon the first absorption. Due to the long excited state lifetimes of the particles (several tens of microseconds), this becomes rather likely in confocal microscopy, even for moderate excitation intensities. The interaction of the two excitons may then result in the formation of a charged nanoparticle via Auger autoionization. The free carrier remaining in the nanoparticle will effectively quench the electronic excitation by energy transfer, thus leading to a so-called dark state. But the return of the charge will neutralize the particle and reactivate the PL. In the present experiment, however, the charge removed from the particle must be trapped in a deep potential well so that recombination is very unlikely and photobleaching occurs rather than long but reversible dark periods. Other photobleaching mechanisms could involve photoinduced chemical modifications of the interface between the crystalline core and the oxide layer leading to dangling bonds or other defects which will quench the PL. Such a kind of bleaching will also be non-reversible.

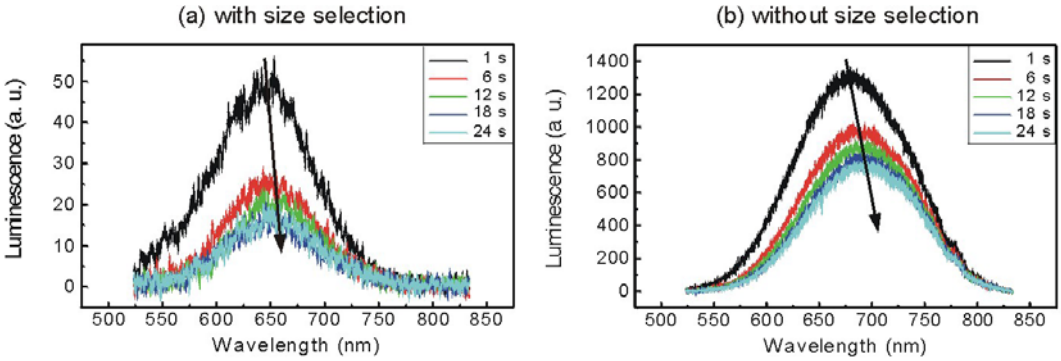

Figure 8. Spectrally resolved bleaching study for a size-selected (a) and non-size-selected (b) sample. With increasing time, the PL intensity decreases and the peak intensity shifts to the red. This is more pronounced for the sample without size selection.

5. Summary and conclusion

CO_2 laser pyrolysis of silane in a gas flow reactor and the extraction of the resulting silicon nanoparticles into a cluster beam apparatus has been shown to provide an excellent means for the production of homogeneous films of non-interacting visible-light-emitting silicon quantum dots. Earlier studies have shown that their PL properties are in perfect agreement with the quantum confinement model, i.e. the PL is the result of the recombination of the electron–hole pair created by the absorption of a UV photon. Other mechanisms involving defects or surface states are not operative in our samples.

Using appropriate masks mounted directly on the substrate, micrometre- and nanometre-sized structures composed of Si nanocrystals were produced. In the present study, we have used commercially available holey carbon films, but the same technique can be applied with any nanostructured mask. Analysis of both masks and deposited films with TEM and AFM reveals nice one-to-one correspondence between them. Nanosized filaments as thin as 33 nm could be imaged on the substrate as grooves in the nc-Si film.

The visible PL of the nc-Si films after excitation with an argon ion laser was recorded with a spatial resolution of 300 nm. Temporally resolved PL decay studies reveal that, under the present conditions, the Si nanocrystals are subjected to photobleaching with a time constant of the order of 1 s. Measuring the PL spectra as a function of time, it was shown that the photobleaching is faster for small Si nanocrystals than for larger ones, giving rise to a spectral red shift of the PL band with progressing time. Moreover, it was found that at least two different photobleaching mechanisms are operative. We tentatively explain the photobleaching by Auger autoionization and photoinduced chemical modification of the interface between crystalline core and surrounding oxide layer.

An interesting application of the deposition technique presented here would be the realization of a Si-nanoparticle-based photonic crystal [16], i.e. a regular structure of columns at the scale of a fraction of the emission wavelength of the nanocrystals. This would allow us to suppress the emission in the plane of the deposit while enhancing the emission perpendicular to the deposit. Combining this structure with two Bragg mirrors [17], it should be possible to build a very efficient silicon-based device (to be pumped by photons). Theoretical and experimental work in this direction is in progress.

Acknowledgments

The authors are grateful to the Deutsche Forschungsgemeinschaft for support in the frame of the Schwerpunktprogramm *Silicon Chemistry* and the Forschergruppe *Laboratory Astrophysics*. GL and DA thank the Alexander-von-Humboldt Foundation and La Region Rhone-Alpes, respectively, for financial support. Fruitful discussions with C von Borczyskowski concerning the optical measurements are gratefully acknowledged.

References

[1] Canham L T 1990 *Appl. Phys. Lett.* **57** 1046
[2] Lehmann V and Gösele U 1991 *Appl. Phys. Lett.* **58** 856
[3] Canham L T 1995 *Phys. Status Solidi* b **190** 9
[4] Cullis A G, Canham L T and Calcott P D J 1997 *J. Appl. Phys.* **82** 909
[5] Brus L E *et al* 1995 *J. Am. Chem. Soc.* **117** 2915
[6] Ehbrecht M, Kohn B, Huisken F, Laguna M A and Paillard V 1997 *Phys. Rev.* B **56** 6958
[7] Ehbrecht M and Huisken F 1999 *Phys. Rev.* B **59** 2975
[8] Ehbrecht M *et al* 1995 *Rev. Sci. Instrum.* **66** 3833
[9] Ledoux G *et al* 2000 *Phys. Rev.* B **62** 15942
[10] Ledoux G *et al* 2001 *Astron. Astrophys.* **377** 707
[11] Ledoux G, Gong J and Huisken F 2001 *Appl. Phys. Lett.* **79** 4028
[12] Huisken F, Kohn B and Paillard V 1999 *Appl. Phys. Lett.* **74** 3776
[13] Ledoux G *et al* 2002 *Mater. Sci. Eng.* C **19** 215
[14] Delerue C, Allan G and Lannoo M 1993 *Phys. Rev.* B **48** 11024
[15] Hofmeister H, Huisken F and Kohn B 1999 *Eur. Phys. J.* D **9** 137
[16] Joannopoulos J D, Meade R D and Winn J N 1995 *Photonic Crystals* (Princeton, NJ: Princeton University Press)
[17] Masenelli B, Gagnaire A, Berthelot L, Tardy J and Joseph J 1999 *J. Appl. Phys.* **85** 3032